Journal of Alloys and Compounds 478 (2009) 154–162

Contents lists available at ScienceDirect

Journal of Alloys and Compounds

journal homepage: www.elsevier.com/locate/jallcom

Influence of the thermal treatment on the microstructure and hardness evolution of 7075 aluminium layers in a hot-rolled multilayer laminate composite

C.M. Cepeda-Jiménez[a,*], M. Pozuelo[b], O.A. Ruano[a], F. Carreño[a]

[a] Department of Physical Metallurgy, CENIM, CSIC, Av. Gregorio del Amo 8, 28040 Madrid, Spain
[b] Department of Materials Science and Engineering, 6531-G Boelter Hall, University of California, Los Angeles, CA 90095-1595, USA

ARTICLE INFO

Article history:
Received 6 October 2008
Received in revised form 11 November 2008
Accepted 14 November 2008
Available online 28 November 2008

Keywords:
Aluminium alloys
Thermomechanical processing
Microstructure
Mechanical properties
EBSD analysis

ABSTRACT

The microstructure and mechanical properties of the Al 7075 alloy present in a hot roll-bonded laminate consisting of Al 7075/Al 2024 layers have been characterized by high resolution electron backscattering diffraction (EBSD) analysis and Vickers microhardness, respectively. The as-rolled deformation structure consisted in lamellar bands aligned parallel to the rolling direction. It was found that a post-rolling tempering at 175 °C/6 h, prior to the T6 treatment has a profound effect on the microstructure and the mechanical properties of the Al 7075 alloy. This tempering reduces the driving force for recrystallization during the usual solution treatment of 30 min that is part of the T6 treatment. The performed procedures favour a more homogeneous precipitation during the following age hardening step and the achievement of a noticeable increase in Vickers microhardness.

1. Introduction

Aluminium alloys are selected for their optimal combination of physical and mechanical properties [1]. Included among these properties are alloy strength, ductility, fatigue resistance, fracture toughness, and corrosion resistance. In order to obtain the desired alloy properties, an appropriate combination of alloy composition and thermal mechanical processing is essential [2]. Great care must be taken in order to ensure that alloys are heat treated correctly. Small deviations from adequate heat treatment may degrade the alloy performance. Additionally, due to the energy stored in the deformed state after conventional processing and the presence of structural heterogeneities, annealing and thermal treatment conditions are critical and non-desired microstructures may form [3–5].

In a previous work, a multilayer laminate composite based on Al 7075 and Al 2024 alloys was developed by hot roll-bonding, resulting in a material with outstanding impact toughness. A detailed mechanical analysis is given in Ref. [6]. The processing was carried out at high temperature, at the solution temperature for the Al 7075 alloy, which is 465 °C. This was followed by a T6 thermal treatment that was applied to generate an efficient and uniform dispersion of precipitates, especially nanosized $MgZn_2$. It is well known that aluminium-based alloys can be strengthened by using solid solution and dispersion hardening. In particular, dispersion hardening is one of the most effective strengthening mechanisms to increase the strength [7]. The conditions of the T6 heat treatment involved solution treatment at 465 °C for 30 min, followed by rapid quenching in water and finally age hardening at 135 °C for 14 h. Additionally, a post-rolling tempering at 175 °C for 6 h prior to the T6 treatment was also carried out to reduce stresses at the interfaces produced by the rolling process. This two-step heat treatment resulted in outstanding toughness of the laminate. However, the influence of these heat treatments on the microstructure and hardness was not studied.

In this work, the main objective is to study the microstructure developed in the Al 7075 alloy during the rolling process applying a deformation $\varepsilon = 0.95$, and its evolution during different T6 treatment conditions with and without prior post-rolling tempering to finally optimize the microstructure and mechanical strength.

2. Experimental procedure

2.1. Materials and processing

The multilayer laminate composite used in the present study is based in 11 alternate layers of Al–Zn 7075 alloy (termed "D") and Al–Cu 2024 (termed "L"), which has been produced by hot roll-bonding and referenced in this work as ADL11. The chemical composition of the two Al alloys is given in weight percentage and is presented in Table 1. The roll-bonding process was carried out at 465 °C in several passes with about 4–8% reduction per pass, with the sample being reheated at 465 °C between the rolling steps, accumulating a total reduction in thickness of 2.3:1, corresponding to an equivalent strain of $\varepsilon = 0.95$ (according to the von Mises criterion). This temperature was selected to be the solution temperature for the 7075 aluminium alloy (D). Additional details about the processing are given elsewhere [6]. The laminate material obtained was in plate form, of about 10 mm in thickness and about 350 mm

* Corresponding author. Tel.: +34 91 5538900; fax: +34 91 5347425.
E-mail address: cm.cepeda@cenim.csic.es (C.M. Cepeda-Jiménez).

0925-8388/$ – see front matter © 2008 Elsevier B.V. All rights reserved.
doi:10.1016/j.jallcom.2008.11.078

Table 1
Chemical composition of the as-received aluminum alloys (weight percent).

Alloy	Si	Fe	Cu	Mn	Mg	Cr	Zn	Ti	Ni
Al 7075 "D"	0.14	0.12	1.36	0.014	2.52	0.22	5.95	0.05	–
Al 2024 "L"	0.17	0.28	4.43	0.62	1.33	0.02	0.04	0.05	0.01

in length and about 60 mm in width. The average thickness of the aluminium layers in the ADL11 laminate composite was about 920 μm.

After hot rolling, the laminate was cooled slowly down to room temperature, and an additional heat treatment was carried out to improve the mechanical properties of the aluminium alloys including the laminate material. Special attention was paid to the Al 7075 alloy due to its superior mechanical strength. The heat treatment that has been deemed as optimum for the 7075 alloy is the T6 treatment. This heat treatment involves solution treatment at 465 °C for a short time interval, followed by rapid quenching in water and final age hardening at 135 °C for 14 h [2]. The time required for the solution heat treatment at 465 °C depends on the type of fabrication procedure, sample thickness and pre-existing microstructure. Thin sheets may require only few minutes. In this study, solution treatment times between 2 and 30 min were considered.

Additionally, the effect of a post-rolling tempering at 175 °C for 6 h [4] prior to the T6 treatment, which has been demonstrated that avoids premature failure at the interfaces [6], has been considered.

2.2. Microstructural determination

The microstructures in the normal direction (ND)–rolling direction (RD) sections of the as-received, as-rolled and thermal treated materials was examined in the SEM using electron backscattering diffraction (EBSD). Particular attention has been paid to the analysis of the aluminium matrix grain structures, grain boundary misorientations distribution and crystallographic textures. Acquisition of EBSD data was carried out using a JEOL JSM 6500F equipment with a field emission gun equipped with a fully automatic HKL Technology EBSD attachment, operating with an acceleration voltage of 20 keV and working distance of 15 mm. The corresponding data processing was carried out using HKL Channel 5 software. Microstructural investigations of the Al 7075 alloy layers were carried out on the midthickness regions of the laminate material. Orientation mapping was performed on a rectangular grid with a step size of 0.3 μm covering an area of 78 (along RD) × 65 (along ND) μm^2. A low-angle grain boundary (LAB) was defined by a misorientation between adjacent grains of $2^\circ < \theta < 15^\circ$, and a high-angle grain boundary (HAB) was defined by $\theta > 15^\circ$. HAB and LAB are shown as black and white lines, respectively, on the maps. Grain boundaries with a misorientation of less than 2° are not included due to the uncertainty in the determination of low-angle misorientations using EBSD. The grain thickness was determined by the linear intercept method in the EBSD maps, counting only HABs ($\theta > 15^\circ$).

Metallographic observation involved methods of standard surface preparation. The samples were electropolished in a 30% nitric acid solution in methanol at −15 °C and 15 V. This is the most favourable preparation of the high strength 7075 aluminium alloy.

2.3. Microhardness test

The mechanical strength of the Al 7075 layers in the ADL11 laminate as a function of different thermal treatments has been evaluated by Vickers microhardness tests. Microhardness measurements were carried out at the laminate interfaces with a Vickers indenter applying a load of 0.1 kp in 15 s. Vickers microhardness values vs. distance to the interface were represented in order to determine the hardness gradient across the interface. The distance to the interface was measured from the indentation centre using image analysis software.

3. Results

3.1. Microstructure

Fig. 1 shows the grain boundary maps obtained from the EBSD measurements of the as-received Al 7075 alloy, as displayed in Fig. 1a; after processing, termed in this study "as-rolled", see Fig. 1b; and in the as-rolled state followed by a post-rolling tempering at 175 °C for 6 h, illustrated in Fig. 1c. In the EBSD maps, the grains are coloured according to crystallographic directions, with red, green and blue colours proportional to the three Euler angles as indicated in the standard stereographic triangle as presented in Fig. 1d.

The as-received material possesses large grains of 20–30 μm in size that are elongated and flattened parallel to the rolling direction, as illustrated in Fig. 1a. The microstructural development during deformation by hot-rolling ($\varepsilon = 0.95$) is shown in the EBSD map of Fig. 1b. After rolling, a lamellar microstructure composed of grains elongated in the rolling direction is formed, and designated as "pancake" structure. Table 2 presents the average grain thicknesses measured from the relative misorientation profile along the vertical lines as shown in the EBSD maps. Additionally, the fraction of high-angle grain boundaries (f_{HAB}) as a function of the different thermal treatment also has been included in Table 2 and it will be commented below. The high-angle grain boundary spacing in the normal direction is reduced from 5.8 μm in the as-received Al 7075 alloy to approximately 3.7 μm in the as-rolled material (Table 2).

In case of the sample post-rolling tempered at 175 °C for 6 h, the microstructure of the specimen, illustrated in Fig. 1c, is quite similar to that of the as-rolled state as shown in Fig. 1b. The grain boundaries and grain interiors appear similar after post-rolling tempering and there is no significant change in grain thickness, of approximately 3.7 μm as depicted in Table 2. The microstructure consists of an array of elongated grains in the rolling direction, with some substructure within the grains.

Fig. 2 shows the EBSD maps corresponding to the Al 7075 after post-rolling tempering at 175 °C for 6 h plus different T6 treatment conditions. The influence of the time at solution temperature of 465 °C on the microstructure evolution has been analyzed. Solution treatment times of 2, 5 and 30 min have been applied and the corresponding microstructures are presented in Fig. 2a–c. The microstructure after post-rolling tempering and solution treatment at 465 °C up to 30 min (Fig. 2a and b) remains practically unchanged, with similar grain thickness than the as-rolled sample (Table 2). The boundaries in the normal direction are usually of low-angle character, and a subgrain structure is clearly observed.

Fig. 3a and b shows the EBSD maps of the Al 7075 alloy in the roll-bonding laminate without post-rolling tempering previous to the T6 treatment. The solution treatment times considered were 5 min (a) and 30 min (b). The deformed microstructures in these samples are similar to those as shown in Fig. 2, comprising lamellar high-angle boundaries aligned parallel to the rolling plane, together with intersecting boundaries which are mainly of low angle. There is a slight tendency to coarsening of the microstructure in comparison with the post-rolling tempered samples subjected to a solution treatment in similar conditions (Table 2). Fig. 3b shows that the deformed grains become slightly larger by solution treating at 465 °C for 30 min without post-rolling tempering, and the mean boundary spacing increased up to about 4 μm. Furthermore, some regions of the microstructure of the Al 7075 alloy are in a more advanced stage of grain coarsening after solution treatment for 30 min, in comparison with the sample that was post-rolling tempered.

3.2. Microtexture

The rolling texture is usually described by a continuous tube of orientations, changing from $\{1\,1\,2\}\langle 1\,1\,1\rangle$ (copper) through $\{1\,2\,3\}\langle 6\,3\,4\rangle$ (S) to $\{1\,1\,0\}\langle 1\,1\,2\rangle$ (brass). By convention, the axis of this tube is called the β-fibre. A second fibre, the α-fibre, extends from $\{1\,1\,0\}\langle 1\,1\,2\rangle$ (brass) to $\{1\,1\,0\}\langle 0\,0\,1\rangle$ (goss) [8]. The homogeneity along the fibres deteriorates as the rolling strain

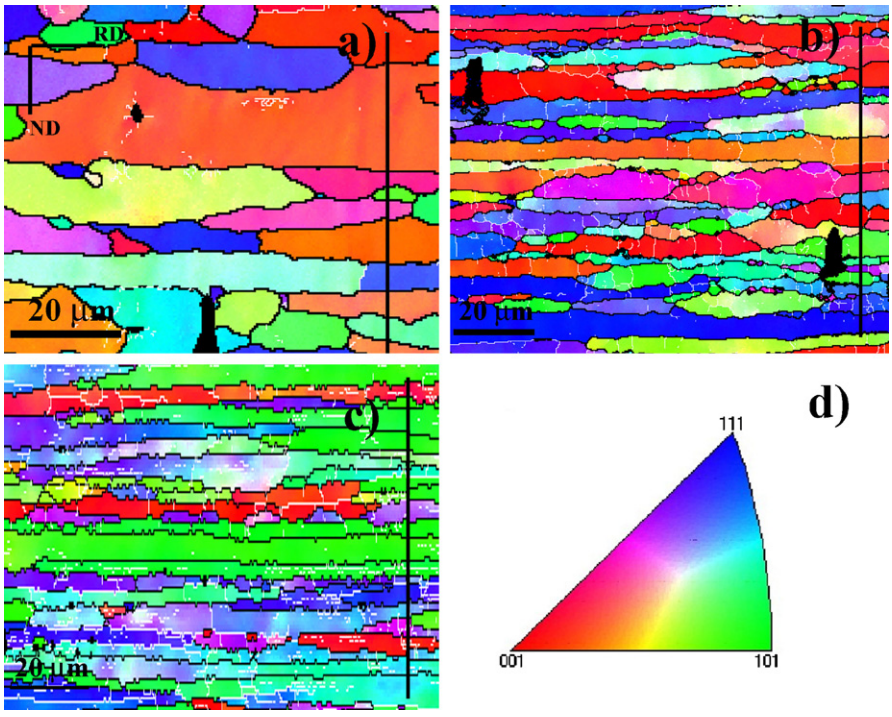

Fig. 1. EBSD maps of a ND–RD section of the Al 7075 alloy: (a) from the as-received sheet; (b) from the as-rolled laminate composite; (c) from the as-rolled and post-rolling tempered laminate for 6 h at 175 °C. (d) Standard stereographic triangle.

Table 2
Microstructural parameters (EBSD) of the Al 7075 layers in the ADL11 laminate composite. Average grain thicknesses measured from the relative misorientation profile along the vertical line shown in Figs. 1–3, and fraction of high-angle grain boundaries, f_{HAB} (%) calculated from Fig. 5.

Thermal treatment	Grain thickness (μm)	Fraction of high-angle grain boundaries, f_{HAB} (%)
As-received Al 7075	5.8	89.5
As-rolled	3.7	70.2
6 h-175 °C	3.7	67.7
6 h-175 °C + 2 min-465 °C + 14 h-133 °C	3.5	75.9
6 h-175 °C + 5 min-465 °C + 14 h-133 °C	3.5	81.4
6 h-175 °C + 30 min-465 °C + 14 h-133 °C	3.7	63.8
5 min-465 °C + 14 h-133 °C	3.9	70.5
30 min-465 °C + 14 h-133 °C	4.0	65.3

increases and this occurs firstly in the α-fibre. Accordingly, if further rolling occurs, deterioration of the β-fibre begins and pronounced peaks are developed. In particular the S component strengthens to become the major component in heavily rolled aluminium.

Orientation data extracted from the EBSD maps of the as-received and as-rolled Al 7075 alloy are plotted in Fig. 4a and b, respectively, as separate {1 1 1} pole figures. Fig. 4c shows the {1 1 1} pole figure corresponding to the β-fibre ideal texture components in as cold-rolled fcc metals [9]. Fig. 4a shows that the as-received material was only weakly textured, and therefore, grains of a wide range of orientations are present. On the other hand, the as-rolled laminate has developed a strong rolling texture, as illustrated in Fig. 4b and c.

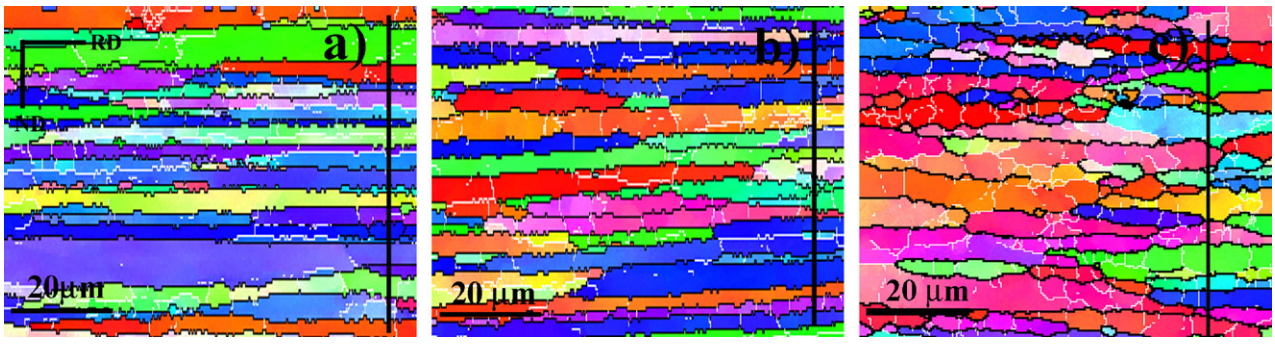

Fig. 2. EBSD maps of a ND–RD section of the Al 7075 alloy in the post-rolling tempered laminate followed by different thermal treatments: (a) 2 min at 465 °C + 14 h at 133 °C; (b) 5 min at 465 °C + 14 h at 133 °C; (c) 30 min at 465 °C + 14 h at 133 °C.

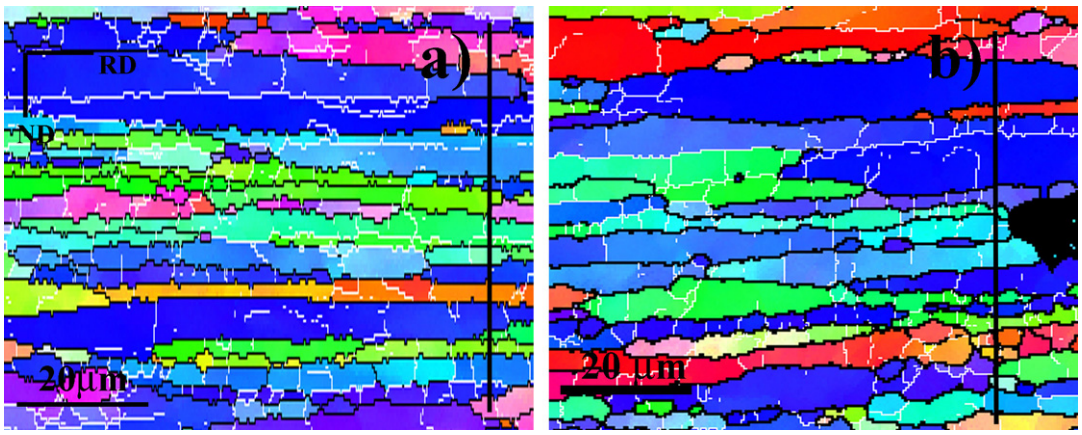

Fig. 3. EBSD maps of a ND–RD section of the Al 7075 alloy in the non-post-rolling tempered laminate followed by different thermal treatments: (a) 5 min at 465 °C + 14 h at 133 °C; (b) 30 min at 465 °C + 14 h at 133 °C.

Additionally, Table 3 presents the percental volume fractions of various texture components after different thermal treatments. As it has been previously commented the as-received 7075 alloy presents a weak rolling texture possessing a considerable amount of other different texture components of about 45.6%. Due to the deformation by rolling, a typical rolling texture comprising variants of ideal orientation components $\{1\,1\,2\}\langle 1\,1\,1\rangle$ (copper), $\{1\,2\,3\}\langle 6\,3\,4\rangle$ (S),$\{1\,1\,0\}\langle 1\,1\,2\rangle$ (brass) and $\{1\,1\,0\}\langle 0\,0\,1\rangle$ (Goss), is well developed in the Al 7075 alloy, with the highest intensity of the S component. Table 3 shows also a decrease in the cube texture after roll-bonding.

The rolling texture is mostly retained after post-rolling tempering, although a comparison with the as-rolled state shows that the $\{0\,0\,1\}\langle 1\,0\,0\rangle$ (cube) texture component is increased and a slight decrease in S and brass texture components occurs.

After different thermal treatments, a decrease in rolling texture components is observed, especially for the longest solution treating time with and without previous post-rolling tempering. In general, the carrying out of a thermal treatment produces a decrease in the S, copper and Goss texture components and, in contrast, an increase in the cube and brass textures occurs. After 30 min of solution treatment with and without post-rolling tempering, an increase in other texture components is observed, which indicates a loss of the main components of the rolling texture. On the other hand, an post-rolling tempering followed by 5 min solution treating corresponds to the thermal treatment with lowest change in the rolling texture.

The grain boundary misorientation distribution and the fraction of high-angle grain boundaries (f_{HAB}) of the as-received Al 7075 alloy, as-rolled sample and all heat treated samples are given in Fig. 5 and Table 2, respectively. The data are derived from the EBSD maps given in Figs. 1–3. In general, all histograms shows two peaks which clearly demonstrated a non-random distribution of grain orientations, as indicated by the superimposed misorientation distribution for randomly orientated grains. In the as-received Al 7075 alloy (Fig. 5a), most of the boundaries are of high angle (>15°) with a f_{HAB} of 89.5%. The deformation introduces a larger number of low-angle boundaries (Fig. 5b) and thus a decrease in f_{HAB} down to 70.2% is observed (Table 2). As it can be seen from Fig. 5c–f, apparently there is no significant change in the fraction of high- and low-angle boundaries after different thermal treatments. Only, a slight increase in the fraction of high-angle boundaries is observed for the sample post-rolling tempered and solutioned for 5 min during the T6 treatment (81.4%) (Fig. 5c and Table 2). The lowest fraction of high-angle boundaries is obtained after extended solution treatment of 30 min with and without post-rolling tempering. Therefore, post-rolling tempering plus solution treatment for 5 min produces a fine-grained microstructure with larger grain misorientations, and a retained rolling texture.

3.3. Microhardness test

Microhardness measurements were carried out across the laminate interfaces after different thermal treatments with and without previous post-rolling tempering. The values are plotted in Fig. 6 and are marked by filled and open symbols, respectively. Additionally, Table 4 presents the average Vickers microhardness values of the different samples taken at a certain distance from the interface. The dashed lines in Fig. 6 indicate the mean microhardness value corresponding to the as-received Al 7075 (188HV) and Al 2024 (138HV) alloys. The Al 7075 layers in the as-rolled laminate composite shows very low microhardness values of 120HV due to the high temperature employed during the processing (465 °C) and the slow cooling rate at room temperature. Post-rolling tempering produces an addi-

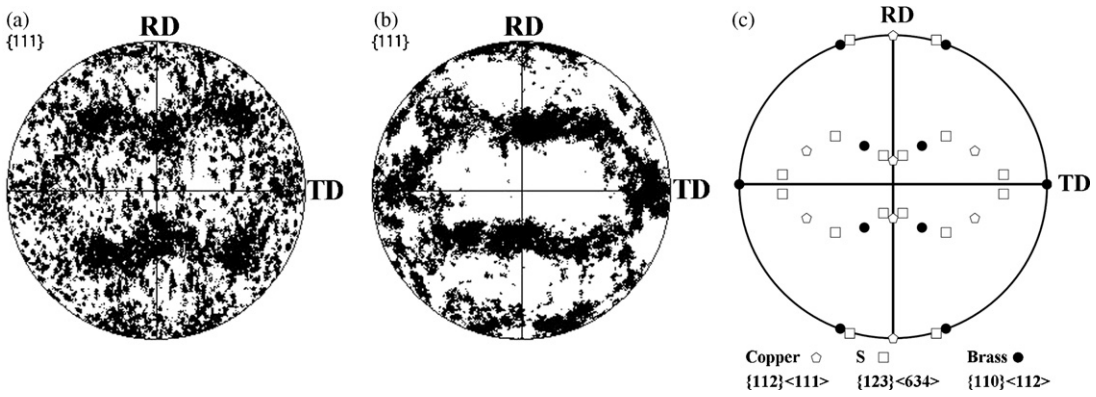

Fig. 4. {1 1 1} pole figures of the Al 7075 alloy: (a) as-received; (b) from the as-rolled laminate; (c) texture components of the β-fibre in rolled fcc metals.

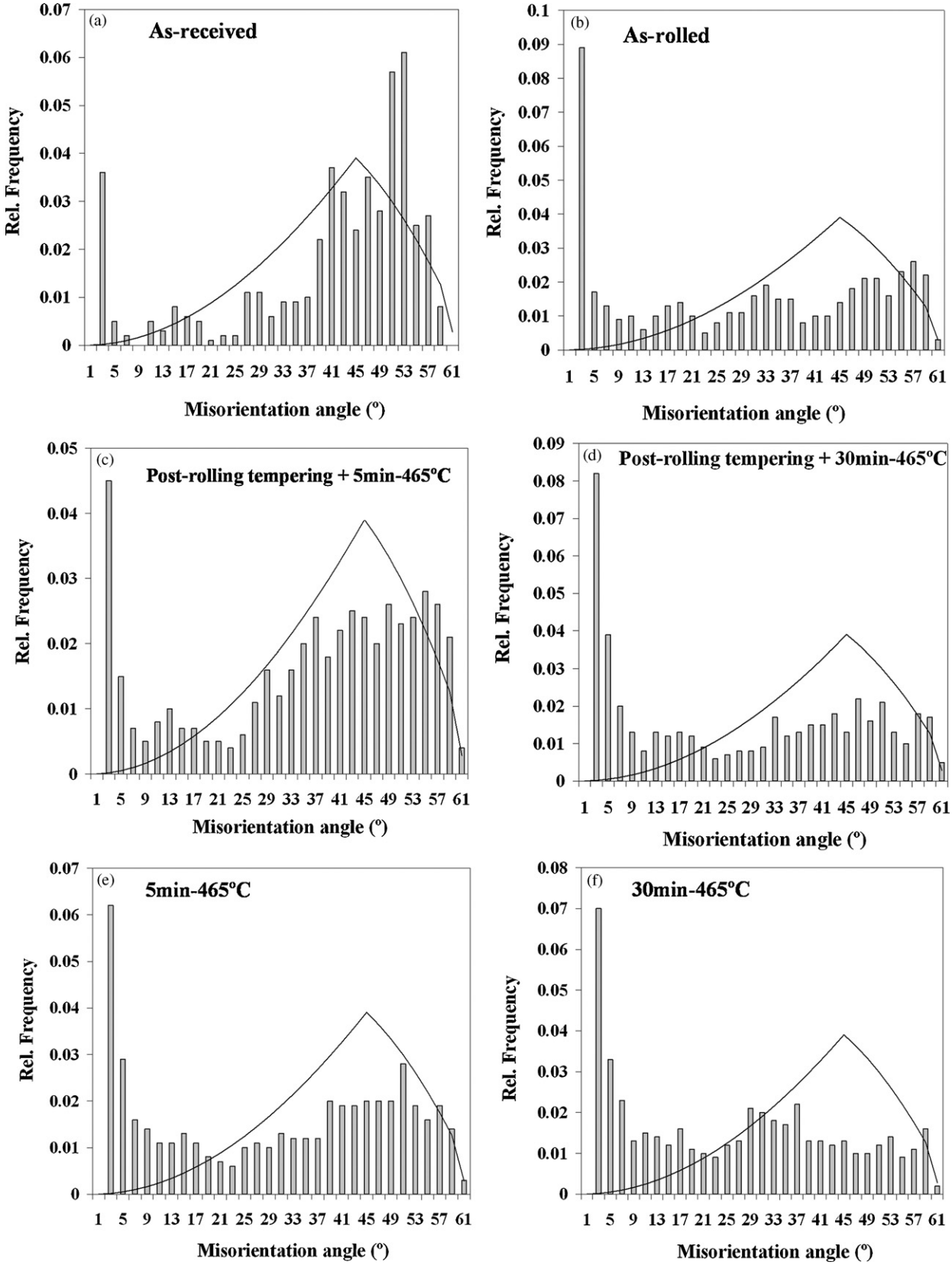

Fig. 5. Misorientation distribution (2–60°) of adjacent grains in Figs. 1–3 with the superimposed theoretical distribution of randomly oriented grains. (a) As-received Al 7075. Al 7075 layers in the laminates: (b) as-rolled; (c) post-rolling tempered +5 min-465 °C + 14 h-133 °C; (d) post-rolling tempered +30 min-465 °C + 14 h-133 °C; (e) non-post-rolling tempered +5 min-465 °C + 14 h-133 °C; (f) non-post-rolling tempered +30 min-465 °C + 14 h-133 °C.

Table 3
Volume percentages of various texture components after different thermal treatments for the Al 7075 alloy in the ADL11 laminate. The given values in the table correspond to grains with orientations within 15° of an ideal texture component.

Thermal treatment	Brass {1 1 0}⟨1 1 2⟩	S {1 2 3}⟨6 3 4⟩	Copper {1 1 2}⟨1 1 1⟩	Goss {1 1 0}⟨0 0 1⟩	Cube {0 0 1}⟨1 0 0⟩	Others
As-received Al 7075	5.6	21.1	6.5	8.8	11.6	46.4
As-rolled	19.7	47.4	11.4	9.0	1.6	10.9
6 h-175 °C	11.6	38.1	17.0	9.8	6.6	16.9
6 h-175 °C + 2 min-465 °C + 14 h-133 °C	16.6	37.1	4.8	9.3	4.2	28
6 h-175 °C + 5 min-465 °C + 14 h-133 °C	32.1	35.8	9.7	8.3	5.2	8.9
6 h-175 °C + 30 min-465 °C + 14 h-133 °C	13.5	23.3	3.8	0.8	6.4	52.2
5 min-465 °C + 14 h-133 °C	25.7	38.0	3.3	3.8	6.3	22.9
30 min-465 °C + 14 h-133 °C	30.5	27.9	4.9	3.6	10.1	23.0

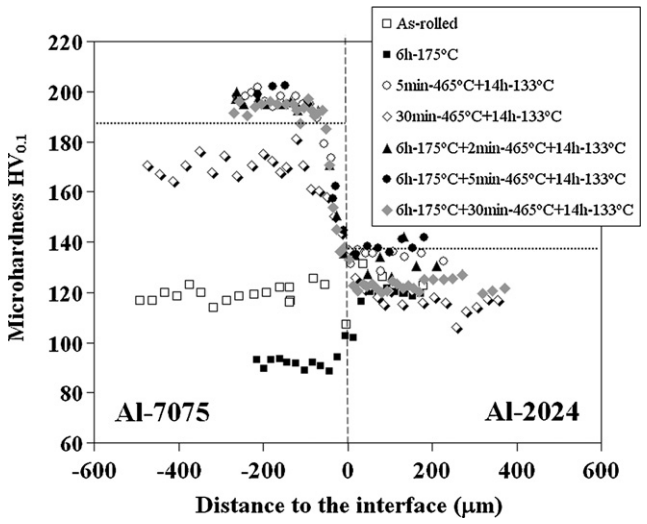

Fig. 6. Vickers microhardness (0.1 kp load; 15 s) of the Al 7075 and Al 2024 alloys subjected to different thermal treatments as a function of the distance to the interface.

tional decrease in the microhardness value to 92HV. All post-rolling tempered and T6 treated samples subjected to different solutioning times show higher microhardness values than the as-received 7075 alloy. The maximum microhardness of 199HV has been achieved for the post-rolling tempered and T6 treated sample with 5 min of solution treatment. On the other hand, the T6 laminate composite without previous post-rolling tempering and solution treatment for 5 min also shows a high microhardness value of 197HV. However, the solution time increase up to 30 min causes a decrease in the microhardness to 171HV of the non-post-rolling tempered sample. Thus, a microstructural change must be responsible for the decrease in microhardness of the non-post-rolling tempered sample subjected to extended solution treatment.

On the other hand, the microhardness value of the Al 2024 layer, after optimum thermal treatment for the Al 7075 alloy of post-rolling tempering plus solution treatment for 5 min, was similar than the Vickers microhardness for the as-received Al 2024 sheet of 138HV. For the rest of conditions and heat treatments analyzed in this study, the microhardness of the Al 2024 layers was lower than that of the as-received material, because the temperatures considered during the processing and subsequent thermal treatments were optimum for the Al 7075 alloy but not for the Al 2024 alloy.

Fig. 7 shows SEM micrographs of the backscattered (BSE) and secondary electrons (SE) modes of Al 7075 layers in the ADL11 laminate heat treated under different temper conditions. The as-rolled sample presents in Fig. 7a a fully covered surface of precipitates, presumably $MgZn_2$ with an average particle size of about 200–300 nm, mostly in needle-like shape. These precipitates are

Table 4
Average Vickers microhardness values (0.1 kp; 15 s) taken from the middle region of the Al 7075 layers in the ADL11 laminate as a function of different thermal treatments (±3 STDEV).

Thermal treatment	HV (Al 7075 "D")
As-received	188
As-rolled	120
6 h-175 °C	92
6 h-175 °C + 2 min-465 °C + 14 h-133 °C	196
6 h-175 °C + 5 min-465 °C + 14 h-133 °C	199
6 h-175 °C + 30 min-465 °C + 14 h-133 °C	194
2 min-465 °C + 14 h-133 °C	198
5 min-465 °C + 14 h-133 °C	197
30 min-465 °C + 14 h-133 °C	171

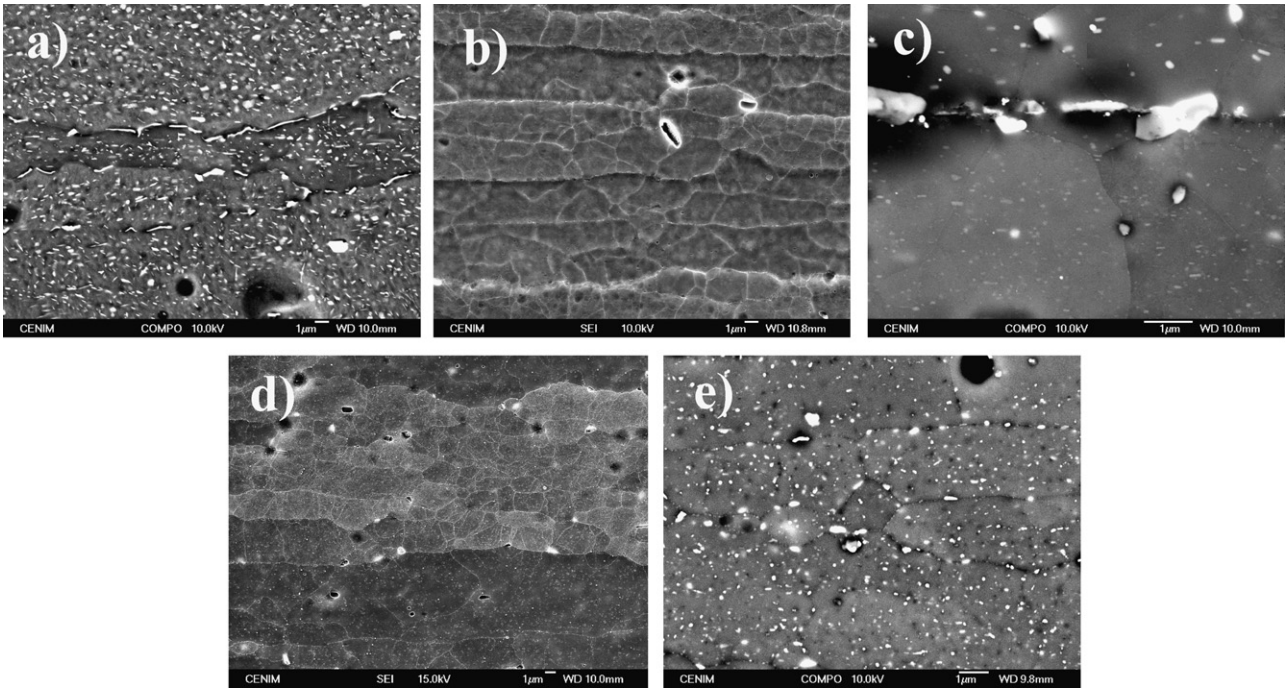

Fig. 7. SEM micrographs of backscattered (a, c, and e) and secondary (b and d) electrons showing the microstructure of the Al 7075 alloy in the laminate material: (a) as-rolled; (b) and (c) post-rolling tempered +30 min-465 °C + 14 h-133 °C; (d) and (e) non-post-rolling tempered +30 min-465 °C + 14 h-133 °C.

present inside the grains and are decorating the grain boundaries. Fig. 7b and c show BSE and SE images of the Al 7075 layers after two-step heat treatment (post-rolling tempering and T6 treatment, having been solutionized for 30 min). The surface at lower magnification (Fig. 7b) appears free of precipitates, which cannot be detected in the SEM due to their small particle sizes. The lamellar structure containing (sub)grains ranged in 1–3 μm size is clearly observed. The microstructure analysis at higher magnification shows in Fig. 7c the presence of nanosize $MgZn_2$ precipitates inside the grains. On the other hand, the secondary electron micrograph of Fig. 7d corresponding to the non-post-rolling tempered sample subjected to solution treatment at 465 °C for 30 min shows some grains in a more advanced stage of coarsening and a subgrain structure is not observed inside these coarsened grains. Furthermore, the BSE micrograph at higher magnification shows in Fig. 7e a homogeneous distribution of rounded precipitates of approximately 50–100 nm in size. These precipitates are considerably bigger than those of the post-rolling tempered sample, and thus responsible for the decrease in mechanical properties of the non-post-rolling tempered sample, according to the Orowan strengthening mechanism. Therefore, the carrying out of an post-rolling tempering plus T6 treatment influences noticeably in the size and a more homogeneous distribution of the precipitates after different heat treatments.

4. Discussion

In the present work, the microstructure of a roll-bonded multilayer laminate composite based on Al 7075 and Al 2024 alloys has been characterized by EBSD technique. Special attention has been paid to the Al 7075 alloy due its higher mechanical strength. Microhardness measurements have been carried out in order to evaluate the mechanical stability under different thermal treatments. Several variants of the T6 treatment together with a previous post-rolling tempering at 175 °C for 6 h were considered. The highest Vickers microhardness has been detected for the post-rolling tempered samples in all analyzed temper conditions.

4.1. Microstructure

The deformation microstructure consisted of lamellar bands aligned to the rolling direction (Fig. 1). These lamellar bands are separated predominantly by HABs. The post-rolling tempering at 175 °C for 6 h does not led apparently to changes in the grain microstructure. Table 2 presents the grain thickness measured by the intercept method along the vertical lines in Figs. 1–3 of the as-rolled sample and under different thermal treatments. The spacing in the normal direction decreases after the roll-bonding process from 5.8 to 3.7 μm, and remains practically constant as a function of the solution treatment time during the T6 treatment. The reduction in the grain thickness is caused by the formation of grain and subgrain boundaries from cell walls by dislocation rearrangements—recovery process—[10] increasing the percentages of low-angle grain boundaries as shown in Table 2. It was found that the elongated grains and the fine-grained structure was remarkably stable at 465 °C for solution treatments up to 30 min. Slight grain coarsening occurring after longer solution treatments of 30 min without post-rolling tempering, as illustrated in Fig. 3 and Table 2. However, for the post-rolling tempered sample a subgrain microstructure is still clearly observed after the longest solution treatment time of 30 min.

It is our assumption that the post-rolling tempering decreases the stored energy during the rolling process. The decrease in driving force for recrystallization hinders the migration of high and low-angle grain boundaries and therefore, grain growth.

It can be concluded that for short solution treatment times of 2–5 min the deformed microstructure remains practically unchanged with post-rolling tempering. For long solution times the post-rolling tempering favours a finer grain structure containing subgrains and, in contrast, without post-rolling tempering a larger grain size of about 4 μm and limited subgrain structure is present.

Furthermore, the “bulk” texture detected at the half thickness of the as-rolled material was measured. The volume percentages of the main texture components recorded within 15% of the ideal orientations are shown in Table 3. The EBSD data analysis

reveals that the undeformed material was only weakly textured and the deformed material developed strong crystallographic textures during rolling. The major texture components are those typically developed during rolling or plane strain deformation of aluminium alloys at elevated temperatures, i.e., the S $\{123\}\langle 634\rangle$, brass $\{011\}\langle 211\rangle$ and copper $\{112\}\langle 111\rangle$ components, with a clear dominance of the S component. The $\{110\}\langle 001\rangle$ (Goss) component was also observed in the as-rolled sample. This component is only common at low to moderate rolling strains and is not sustained after high strains [9]. The strong rolling texture is progressively reduced with increasing solution treatment time, especially the S and copper texture components. The fraction of the cube texture component increases with the solution treatment time at 465 °C, especially for the non-post-rolling tempered sample that was solution treated for 30 min during the T6 temper. The $\{100\}\langle 001\rangle$ cube orientation has been reported as the recrystallization texture in many aluminium alloys [8,10].

Hence, during solution treatment for a longer time period of 30 min, discontinuous recrystallization takes place, generating a coarse grained microstructure of about 4 μm in thickness, weakening the rolling texture and appearing a cube texture component. The grain coarsening is especially notable for the non-post-rolling tempered sample whereby the (sub)grain microstructure has been considerably removed and a small number of grains grow rapidly to produce coarse grains, of 5–10 μm in size, see Fig. 3b.

4.2. Vickers microhardness test

Grain refinement is not the main contributor to the high strength of the Al 7075 alloy [11]. According to the strengthening mechanism of age hardened aluminum alloys, an efficient distribution and a higher density of precipitates leads to a higher strength according to the Orowan mechanism. The microhardness of as-received Al 7075 alloy decreases during the roll-bonding process and more markedly after subsequent post-rolling tempering, as illustrated in Fig. 6. However, the microstructure of as-rolled laminate materials was finer than of the as-received Al 7075 alloy. This decrease in microhardness is a consequence of the slow cooling rate after rolling originating coarse precipitates and second phase particles. Additionally, during the post-rolling tempering procedure at 175 °C, an additional coarsening of these precipitates plus recovery of internal stresses stored during the rolling process occurs, which decreases even more the mechanical strength. This result highlights the crucial importance of precipitation hardening in this kind of age hardened alloys. From microstructural observations, see Fig. 7, we can affirm that the coarsened precipitates, as illustrated in Fig. 7a, in the as-rolled sample are responsible for the low microhardness value obtained in the as-rolled and in the as-rolled plus post-rolling tempered states.

Hence, an appropriate thermal treatment warrants the high hardness of the Al 7075 alloy as presented in Fig. 6. All samples post-rolling tempered and T6 treated at different solution times showed higher microhardness value than the as-received Al 7075 alloy. The maximum Vickers hardness value of 199HV was obtained for the post-rolling tempered sample solutionized for 5 min. Finally, non-post-rolling tempered samples which were solution treated at 2 and 5 min also showed higher microhardness than the as-received material. However, the increase in the solution treatment time up to 30 min decreases noticeably the mechanical strength of the non-post-rolling tempered Al 7075 alloy, see Table 4 and Fig. 6. Regarding this hardness decrease, a coarsening of both second phase particles and matrix grains was observed in the non-post-rolling tempered sample solutionized for 30 min at 465 °C, see Fig. 7d and e, in comparison with the sample post-rolling tempered and heat treated in similar conditions, illustrated in Fig. 7b and c, whereby finer precipitates and a subgrain microstructure were observed. In this study, the optimum thermal treatment to obtain maximum Vickers microhardness consisted of post-rolling tempering at 175 °C for 6 h followed by T6 temper involving solution treatment for 5 min.

It is our contention that the time required for solution treatment during T6 tempering procedure depends therefore on the prior microstructure and second-phase particle distribution after rolling. The rate of dissolution during T6 will be different as a function of the particle size. Thus, the main consideration is that the coarsened particles after post-rolling tempering extends the stability range during the subsequent thermal treatments. Accordingly, post-rolling tempering produces a pronounced distribution of coarsened precipitates which require longer solution times. This gives more stability to the deformed microstructure at high temperatures. For this reason, both lower fraction of the cube texture component which is associated with discontinuous recrystallization and more homogeneous (sub)grain microstructure for extended solution treatment (30 min) have been observed for the post-rolling tempered samples, as shown in Table 3 and Fig. 7. Additionally, it can be assumed that the internal stresses developed upon quenching during the following T6 treatments will be more homogeneously distributed in a finer-grained microstructure like that of the post-rolling tempered samples. Thus, a finer subgrain microstructure for the post-rolling tempered and solution treated for 30 min sample will favour a more efficient precipitation hardening resulting in a higher microhardness. Therefore, particles which are finer and closely spaced leads to a higher strength as deduced from the Orowan mechanism.

In summary, considering the microstructure and the Vickers hardness measurements, it can be concluded that for a 30 min solution treatment the material without post-rolling temper shows a coarse microstructure and low hardness. In contrast, a post-rolling tempering procedure prior to solution treatment increases the thermal stability, producing a finer (sub)grain microstructure and an optimum precipitation hardening.

5. Conclusions

The microstructure and mechanical properties evolution of the Al 7075 layers in a roll-bonded laminate composite with a total thickness reduction of 2.3:1, equivalent to a von Mises strain of $\varepsilon = 0.95$, after different heat treatments has been characterized by EBSD analysis and Vickers microhardness. A post-rolling tempering treatment (6 h at 175 °C) prior to the T6 treatment has been considered for its beneficial effects removing stresses at the interfaces and improving the laminate toughness. The influence of the solution treatment time with and without prior post-rolling tempering has been analyzed. The main conclusions of this study are as follows:

1. The deformation structure of Al 7075 alloy in the as-roll-bonded laminate contains lamellar bands aligned parallel to the rolling direction. During deformation the typical "β-fibre" rolling texture is developed.
2. The high-angle grain boundary spacing decreases after processing to about 3.7 μm. This grain thickness remains constant after T6 treatment involving solution treatment up to 30 min at 465 °C. The post-rolling tempered +T6 sample maintains a more homogeneous microstructure than the non-post-rolling tempered sample which shows coarsened grains.
3. Post-rolling tempering and T6 treatment for all solution times considered in this study produces an important increase in Vickers microhardness of the Al 7075 alloy.
4. The thermal stability induced by the post-rolling tempering prior to final T6 treatment is due to coarsened precipitates that stabilize the fine substructure during following thermal treatments.

Additionally, the post-rolling tempering decreases the stored energy during hot rolling, reduces the driving force for nucleation and grain growth and favours a more homogeneous precipitation hardening.

5. Post-rolling tempering at 175 °C for 6 h followed by a T6 treatment involving 5 min solution treatment time was optimum to improve the Vickers hardness of the Al 7075 alloy, retaining the rolling microstructure and optimizing precipitation hardening.

Acknowledgements

Financial support from CICYT (Projects MAT2003-01172 and MAT2006-11202) is gratefully acknowledged. C.M. Cepeda-Jiménez thanks the Spanish National Research Council (CSIC) for a I3P contract.

References

[1] D Wang, Z.Y. Ma, J. Alloys Comp. (2008), doi:10.1016/j.jallcom.2008.01.137.
[2] J.E. Hatch (Ed.), Aluminium: Properties and Physical Metallurgy, ASM, Metals Park, OH, 1984.
[3] W.J. Kim, J.K. Kim, H.K. Kim, J.W. Park, Y.H. Jeong, J. Alloys Comp. 450 (2008) 222–228.
[4] N. Kamikawa, N. Tsuji, X. Huang, N. Hansen, Acta Mater. 54 (2006) 3055–3066.
[5] L. Hadjadj, R. Amira, D. Hamana, A. Mosbah, J. Alloys Comp. 462 (2008) 279–283.
[6] C.M. Cepeda-Jiménez, M. Pozuelo, J.M. García-Infanta, O.A. Ruano, F. Carreño, Metall. Mater. Trans 40A (2009) 69–79.
[7] R.K. Islamgaliev, N.F. Yunusova, I.N. Sabirov, A.V. Sergueeva, R.Z. Valiev, Mater. Sci. Eng. A 319–321 (2001) 877–881.
[8] F.J. Humphreys, M. Hatherly, Recrystallization and Related Annealing Phenomenon, 2nd ed., Elsevier, Oxford, UK, 2004, pp. 70–71 (Chapter 3).
[9] M.Z. Quadir, O. Al-Buhamad, L. Bassman, M. Ferry, Acta Mater. 55 (2007) 5438–5448.
[10] H. Jazaeri, F.J. Humphreys, Acta Mater. 52 (2004) 3239–3250.
[11] Y.H. Zhao, X.Z. Liao, Z. Jin, R.Z. Valiev, Y.T. Zhu, Acta Mater. 52 (2004) 4589–4599.